2 Image Registration

Separate images of related objects are compared or aligned by at least implicitly conceiving a correspondence between like points. For example, two given images may be of a single patient at different times, such as during a mammography examination involving repeated imaging after the injection of a contrast agent [28]. On the other hand, the images may be of a single patient viewed by different imaging modalities, such as by magnetic resonance and computerized tomography to provide complementary information for image-guided surgery [8]. In fact, images of two separate patients may even be compared to evaluate the extent of pathology of one in relation to the other [30]. Similarly, an image of a patient may be compared to an idealized atlas in order to identify or segment tissue classes based upon a detailed segmentation of the atlas [30]. When an explicit coordinate transformation connecting like points is constructed, images are said to be *registered*. When a parameterized transformation permits images to be morphed one to the other, images are said to be *interpolated*. Since many applications involve the processing of sets as opposed to pairs of images, it is also of interest to consider methods for registering and interpolating image sequences.

Since the term registration is often used rather loosely in the context of its applications, it may be useful to elaborate on the above description of what registration is by stating what it is not. Note that by manipulating intensities alone, it is possible to warp or morph one image to another without having an explicit coordinate transformation identifying like image points. Thus image registration is not image morphing, but can be used for such an application. Similarly, a *continuous* warping of one image to another can be achieved without registration, but a parameterized coordinate transformation can be used to interpolate between images. Also, when complementary information in separate imaging modalities is superimposed, images are said to be *fused*. Since fusion too can be achieved by manipulating intensities alone, fused images need not be registered, but rather *can* be fused by registration.

In order to compute a transformation which matches given images, two main ingredients are combined. First, there must be a measure of image similarity to quantify the extent to which a prospective transformation has achieved the matching goal [8]. Secondly, owing to the ill-posed nature of the registration problem, very pathological transformations are possible but not desired, and therefore a measure of transformation regularity is required [24]. Typically one determines the desired transformation by minimizing an energy functional consisting of a weighted sum of these two measures.

The simplest image similarity measure is the sum of squared intensity differences, which is natural when images are related by a simple misalignment. Statistical measures have also been employed, and the correlation coefficient has been recognized as ideal when the intensities of the two images are related by a linear rescaling [31]. Also, the adaptation of thermodynamic entropy for information theory has suggested mutual information as an image similarity measure [23] [32], and a heuristically based normalized mutual information has been found to work very well in practice [29]. In [33] it is found in practice that highly accurate registrations of multi-modal brain images can be achieved with information-theoretic measures. Nevertheless, as recognized in [27], mutual information contains no local spatial information, and random pixel perturbations leave underlying entropies unchanged. Higher order entropies including probabilities of neighboring pixel pairs can be employed to achieve superior results for non-rigid registration [27]; however, the message is that local spatial information in an image similarity measure is advantageous. In [4] Gauss maps are used to perform morphological, i.e., contrast invariant, image matching. Image level sets are also matched in [5] by using a Mumford-Shah formulation for registration. Higher order derivatives of the optical flow equation residual are penalized for an image similarity measure in [34] to obtain optical flows which do not require image structures to maintain a temporally constant brightness. In [2], the optical flow equation residual is replaced by a contrast invariant similarity measure which aligns level sets. In [16] the constant brightness assumption is circumvented without differential formulations by simply

composing intensities with scaling functions.

The simplest approach to achieving regularity in a registration transformation is to use a low-dimensional parameterization. Before computing a very general type of registration transformation, many practitioners often consider first how well one of two natural classes of parameterized transformations manage to match given images: rigid and affine transformations. A rigid transformation is a sum of a translation and a rotation. An affine transformation is a sum of a translation and a matrix multiplication which is no longer constrained to be conformal or isometric. A registration or interpolation method may be called *generalized rigid* or *generalized affine* if it selects a rigid or an affine transformation, respectively, when one fits the given images [17]. The motivation for considering rigid or affine transformations, and generalizations thereof, lies in their applicability in two important categories of biomedical imaging. First, generalized rigid registration and interpolation are of particular interest, for instance, to facilitate medical examination of dynamic imaging data because of the ubiquity of rigid objects in the human body. Secondly, generalized affine registration and interpolation are of particular interest, for instance, for object reconstruction from histological data since histological sections may be affine deformed in the process of slicing. A leading application and demand for non-rigid registration is for mammographic image sequences in which tissue deformations are less rigid and more elastic [28]. This observation has motivated the development of registration methods based on linear elasticity [6], [26]. Some authors relax rigidity by constraining transformations to be conformal or isometric [11]. Others employ a local rigidity constraint [21] or allow identified objects to move as rigid bodies [22].

2.1 Variational Framework

Image registration and interpolation can be visualized using the illustration in Fig. 1 for 2D images, in which two given images I_0 and I_1 are situated respectively on the front and back

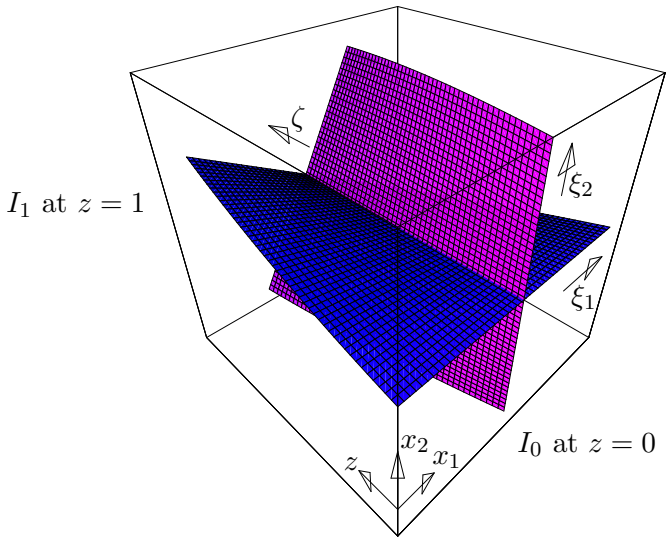

Figure 1: The domain Q with 2D images I_0 and I_1 on the front and back faces Ω_0 and Ω_1, respectively. Curvilinear coordinates are defined to be constant on trajectories connecting like points in I_0 and I_1.

faces of a box $Q = \Omega \times (0,1)$ where a generic cross section of Q is denoted by $\Omega = (0,1)^N$. In particular, the front and back faces of Q are denoted by Ω_0 and Ω_1, on which I_0 and I_1 are situated respectively. The rectangular spatial coordinates in Ω are denoted by $\boldsymbol{x} = (x_1, \ldots, x_N)$ and the depth or temporal coordinate by z.

The surfaces shown in Fig. 1 are surfaces in which all but one of the curvilinear coordinates $\boldsymbol{\xi} = (\xi_1, \ldots, \xi_N)$ are constant, and the intersection of these surfaces represents a trajectory through Q connecting like points in I_0 and I_1. The coordinates $\boldsymbol{\xi}(\boldsymbol{x}, z)$ are initialized in Ω_0 so that $\boldsymbol{\xi}(\boldsymbol{x}, 0) = \boldsymbol{x}$ holds, and therefore the displacement vector within Q is $\boldsymbol{d}(\boldsymbol{x}, z) = \boldsymbol{x} - \boldsymbol{\xi}(\boldsymbol{x}, z)$.

The curvilinear coordinate system is completed by parameterizing a trajectory in the depth direction according to $\zeta = z$. Thus, a trajectory emanating from the point $\boldsymbol{\xi} \in \Omega_0$ is denoted by $\boldsymbol{x}(\boldsymbol{\xi}, \zeta)$. The coordinates in Ω_1 of the finite displacement from coordinates $\boldsymbol{\xi}$ in Ω_0 are written as $\boldsymbol{x}(\boldsymbol{\xi}) = \boldsymbol{x}(\boldsymbol{\xi}, 1)$. For those points in Q situated on a trajectory joined to Ω_1 but not necessarily to Ω_0, let $\boldsymbol{y} = (y_1, \ldots, y_N)$ and $\boldsymbol{\eta} = (\eta_1, \ldots, \eta_N)$ be the counterparts to $\boldsymbol{x}$ and $\boldsymbol{\xi}$ defined so that $\boldsymbol{\eta}(\boldsymbol{y}, 1) = \boldsymbol{y}$ holds in Ω_1; thus, a trajectory emanating from the point $\boldsymbol{\eta} \in \Omega_1$ is denoted by $\boldsymbol{y}(\boldsymbol{\eta}, \zeta)$, and the finite displacement from Ω_1 to Ω_0 is written as $\boldsymbol{y}(\boldsymbol{\eta}) = \boldsymbol{y}(\boldsymbol{\eta}, 0)$. A trajectory tangent is given by $(u_1, \ldots, u_N, 1)$ in terms of the optical flow defined as $\boldsymbol{u} = (u_1, \ldots, u_N) = \boldsymbol{x}_\zeta$. Since it is not assumed that every point in Ω_0 finds a like point in Ω_1, let the subsets of Ω_0 and Ω_1 with respect to which trajectories extend completely through the full depth of Q be denoted respectively by $\Omega_0^{\mathrm{c}} = \{\boldsymbol{\xi} \in \Omega_0 : \boldsymbol{x}(\boldsymbol{\xi}, \zeta) \in Q, 0 < \zeta < 1\}$ and $\Omega_1^{\mathrm{c}} = \{\boldsymbol{\eta} \in \Omega_1 : \boldsymbol{y}(\boldsymbol{\eta}, \zeta) \in Q, 0 < \zeta < 1\}$. For those trajectories extending incompletely through Q define $\Omega_0^{\mathrm{i}} = \Omega_0 \backslash \Omega_0^{\mathrm{c}}$ and $\Omega_1^{\mathrm{i}} = \Omega_0 \backslash \Omega_1^{\mathrm{c}}$.

To perform image registration using a finite displacement field $\boldsymbol{x}$, a functional of the following form can be minimized:

$$J(\boldsymbol{x}) = \mathcal{S}(\boldsymbol{x}) + \mathcal{R}(\boldsymbol{x}) \tag{2.1}$$

where $\mathcal{S}(\boldsymbol{x})$ is an image similarity measure depending upon the given images I_0 and I_1 and $\mathcal{R}(\boldsymbol{x})$ is a regularity measure of the transformation $\boldsymbol{x}$. To perform image registration and interpolation using an optical flow field $\boldsymbol{u}$ and an interpolated intensity I, a functional of the following form can be minimized:

$$J(\boldsymbol{u}, I) = \mathcal{S}(\boldsymbol{u}, I) + \mathcal{R}(\boldsymbol{u}) \tag{2.2}$$

where the intensity field I is constrained by the boundary conditions:

$$I(\boldsymbol{x}, 0) = I_0(\boldsymbol{x}), \quad I(\boldsymbol{x}, 1) = I_1(\boldsymbol{x}) \tag{2.3}$$

and $\mathcal{S}(\boldsymbol{u}, I)$ quantifies the variation of intensity I in the flow direction $(\boldsymbol{u}, 1)$ while $\mathcal{R}(\boldsymbol{x})$ is a regularity measure of the optical flow $\boldsymbol{u}$. Trajectories through the domain Q are defined by integrating the optical flow under boundary conditions, i.e., by solving:

$$\boldsymbol{x}(\boldsymbol{\xi}, \zeta) = \boldsymbol{\xi} + \int_0^\zeta \boldsymbol{u}(\boldsymbol{x}(\boldsymbol{\xi}, \rho), \rho) d\rho, \qquad \boldsymbol{\xi} \in \Omega_0, \quad \zeta \in [0, 1]. \tag{2.4}$$

and a similar equation for $\boldsymbol{y}(\boldsymbol{\eta}, \zeta)$ with $\boldsymbol{\eta} \in \Omega_1$ and $\zeta \in [0, 1]$. A registration is given by the coordinate transformation $\boldsymbol{x}(\boldsymbol{\xi}, 1)$ and by the inverse transformation $\boldsymbol{y}(\boldsymbol{\eta}, 0)$. The given images I_0 and I_1 are interpolated by the intensity I.

2.2 Similarity Measures

The simplest similarity measure involves the squared differences $[I_0(\boldsymbol{\xi}) - I_1(\boldsymbol{x}(\boldsymbol{\xi}))]^2$ over Ω_0^{c}. However, as discussed in detail in [17], Ω_0^{c} depends upon $\boldsymbol{x}(\boldsymbol{\xi})$. To avoid having to differentiate the domain with respect to the displacement for optimization, it is assumed that the images I_0 and I_1 can be continued in $\boldsymbol{R}^N$ by their respective *background* intensities, I_0^∞ and I_1^∞, which are understood as those intensities for which no active signal is measured. For simplicity, it is assumed here that the background intensities are zero. With such continuations, a similarity measure can be defined in terms of the sum of squared differences as follows:

$$\mathcal{S}_1(\boldsymbol{x}) = \int_{\Omega_0} [I_0(\boldsymbol{\xi}) - I_1(\boldsymbol{x}(\boldsymbol{\xi}))]^2 \, d\boldsymbol{\xi} \tag{2.5}$$

where here and below $I_1(\boldsymbol{x}(\boldsymbol{\xi}))$, $\boldsymbol{\xi} \in \Omega_0^{\mathrm{i}}$ is understood as zero. So that $\mathcal{S}_1$ is independent of the order in which images are given, a similar integral over Ω_1 may be added in (2.5) in which $I_0(\boldsymbol{y}(\boldsymbol{\eta}))$, $\boldsymbol{\eta} \in \Omega_1^{\mathrm{i}}$ is understood as zero.

As illustrated in Fig. 2 the finite displacements discussed above in connection with (2.5)

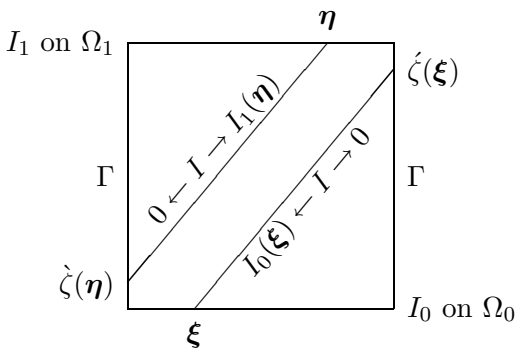

Figure 2: $\acute{\zeta}(\boldsymbol{\xi})$ and $\grave{\zeta}(\boldsymbol{\eta})$ denote the ζ coordinates at which trajectories emanating respectively from $\boldsymbol{\xi} \in \Omega_0^{\mathrm{i}}$ and $\boldsymbol{\eta} \in \Omega_1^{\mathrm{i}}$ meet Γ.

can be written equivalently in terms of trajectories passing at least partly through Q and some impinging upon the side of the box:

$$\Gamma = \partial Q \backslash \{\Omega_0 \cup \Omega_1\} \tag{2.6}$$

The corresponding intensity differences can be written equivalently in terms of integrals of $[dI/d\zeta]^2$ for an intensity I satisfying the boundary conditions (2.3) as well as those illustrated in Fig. 2:

$$I = 0 \text{ on } \Gamma. \tag{2.7}$$

Once such integrals of $[dI/d\zeta]^2$ are transformed from the *Lagrangian* (trajectory following) form to the *Eulerian* (local) counterpart, $dI/d\zeta = \nabla I \cdot \boldsymbol{u} + I_z$, and transformation Jacobians such as $1/\det[\nabla_{\boldsymbol{\xi}} \boldsymbol{x}]$ are neglected, the following penalty on the optical flow equation residual [15] is obtained:

$$\mathcal{S}_2(\boldsymbol{u}, I) = \int_Q [\nabla I \cdot \boldsymbol{u} + I_z]^2 \, d\boldsymbol{x} dz \tag{2.8}$$

subject to the boundary conditions (2.3) and (2.7).

To circumvent a constant brightness condition along trajectories, which in the present context involves minimizing the variation of the intensity I along a trajectory, the similarity may be defined in terms of intensity derivatives as follows [34]:

$$\mathcal{S}_3(\boldsymbol{u}, I) = \int_Q [\nabla |\nabla I| \cdot \boldsymbol{u} + |\nabla I|_z]^2 \, d\boldsymbol{x} dz \tag{2.9}$$

To avoid the use of derivatives, the given data may instead be composed with scaling functions so that the intensity I in (2.8) is constrained by the following modification of (2.3):

$$I = \sigma_0(I_0) \text{ on } \Omega_0, \quad I = I_1 \text{ on } \Omega_1 \tag{2.10}$$

in which only I_0 is scaled, and I_1 may be scaled similarly [16]. Furthermore, both of the given images may be scaled reciprocally in order that the registration be independent of image order [16].

The simplest statistical image similarity measure is the correlation coefficient:

$$\mathcal{S}_4(\boldsymbol{x}) = \int_{\Omega_0} \left[\frac{I_0(\boldsymbol{\xi}) - \mu(I_0)}{\sigma(I_0)} \right] \left[\frac{I_1(\boldsymbol{x}(\boldsymbol{\xi})) - \mu(I_1 \circ \boldsymbol{x})}{\sigma(I_1 \circ \boldsymbol{x})} \right] d\boldsymbol{\xi} \tag{2.11}$$

where $\mu(I_0) = \int_{\Omega_0} I_0 dx / \mathrm{meas}(\Omega_0)$ and $\sigma(I_0) = \mu([I_0 - \mu(I_0)]^2)$ denote the mean value and variance of I_0 respectively. So that $\mathcal{S}_4$ is independent of the order in which images are given, a similar integral over Ω_1 may be added in (2.11) as with (2.5). The similarity measures (2.5) and (2.11) coincide when they are restricted to pure translation [24]. A more complex statistical image similarity measure is the mutual information:

$$\mathcal{S}_5(\boldsymbol{x}) = H(I_0) + H(I_1 \circ \boldsymbol{x}) - H(I_0, I_1 \circ \boldsymbol{x}) \tag{2.12}$$

where, for images taking values in the interval $[0,1]$, the entropy $H(A)$ of image A and the joint entropy $H(A,B)$ of images A and B are given by:

$$\begin{aligned} H(A) &= -\int_0^1 p(A=a)\log[p(A=a)]da \\ H(A,B) &= -\int_0^1\int_0^1 p(A=a,B=b)\log[p(A=a,B=b)]dadb \end{aligned} \tag{2.13}$$

Here, $p(A=a)$ denotes the probability that the image A assumes the intensity a, and $p(A=a,B=b)$ denotes the probability that the images A and B assume the intensities a and b simultaneously. So that $\mathcal{S}_5$ is independent of the order in which images are given, the sum $H(I_0\circ\boldsymbol{y})+H(I_1)-H(I_0\circ\boldsymbol{y},I_1)$ may be added in (2.12) as with (2.5) and (2.11). For a simple example of mutual information, let A and B be the following 2×2 images:

$$A=\begin{array}{|c|c|}\hline 0&0\\\hline 1&1\\\hline\end{array}\quad B=\begin{array}{|c|c|}\hline 0&1\\\hline 0&1\\\hline\end{array} \tag{2.14}$$

So the intensity values are $\{a_i\}=\{0,0,1,1\}=\{b_j\}$ and their probabilities are $p(A=a_i)=\frac{1}{2}=p(B=b_j)$. Also, there are precisely four intensity pairs $\{(0,0),(0,1),(1,0),(1,1)\}$, each with probability $p(A=a_i,B=b_j)=\frac{1}{4}$. The entropies of the two images are the same, $H(A)=H(B)=\log(2)$. The joint entropy is $H(A,B)=\log(4)$, which is larger than the joint entropy of A with itself, $H(A,A)=\log(2)$. Thus, a transformation which rotates image B to be aligned with the image A would minimize the mutual information. Note that this similarity measure operates purely on intensity values and on pairs of intensity values, and it involves no local spatial information. Such spatial information can be incorporated by defining higher order entropies involving probabilities of neighboring pixel pairs [27]. On the other hand, the variational treatment of (2.12) and variations of it are more complicated than that of similarity measures such as (2.5) with an explicit spatial orientation [24].

When finitely many clearly matching points are identified manually, or else from particular features found in the images I_0 and I_1, these landmarks:

$$\boldsymbol{\mathcal{E}}_\ell(\boldsymbol{x})=\boldsymbol{x}(\boldsymbol{\xi}_\ell)-\boldsymbol{x}_\ell=0,\quad \ell=1,\ldots,L \tag{2.15}$$

may be used as constraints in the optimization process for determining the registration or interpolation. On the other hand, these landmarks may be used exclusively to determine a parametric registration by minimizing the sum of squared differences of the landmark residuals [9]:

$$\mathcal{S}_6(\boldsymbol{x})=\sum_{\ell=1}^{L}|\boldsymbol{x}_\ell-\boldsymbol{x}(\boldsymbol{\xi}_\ell)|^2. \tag{2.16}$$

2.3 Regularity Measures

The most easily determined registrations are those which are parametric and low-dimensional. For instance, a transformation $\boldsymbol{x}$ could be computed as a combination of thin plate spline functions:

$$\boldsymbol{x}(\boldsymbol{\xi})=\sum_{m=1}^{N+1}\boldsymbol{\alpha}_m P_m(\boldsymbol{\xi})+\sum_{\ell=1}^{L}\boldsymbol{\beta}_\ell U(\boldsymbol{\xi}-\boldsymbol{\xi}_\ell) \tag{2.17}$$

where $U(\boldsymbol{\xi})=|\boldsymbol{\xi}|^{4-N}\log|\boldsymbol{\xi}|$ for N even (or $U(\boldsymbol{\xi})=|\boldsymbol{\xi}|^{4-N}$ for N odd) and $\{P_m\}$ is a basis for linear functions. The transformation in (2.17) which minimizes the following regularity measure:

$$\mathcal{R}_1(\boldsymbol{x})=\sum_{|\alpha|=2}\frac{2!}{\alpha!}\int_{\Omega_0}|\partial^\alpha_{\boldsymbol{\xi}}\boldsymbol{x}|^2 d\boldsymbol{\xi} \tag{2.18}$$

under the constraints in (2.15) is given by solving systems of the form [24]:

$$\begin{pmatrix} K & B^{\mathrm{T}} \\ B & 0 \end{pmatrix} \begin{pmatrix} \bar{\boldsymbol{\alpha}} \\ \bar{\boldsymbol{\beta}} \end{pmatrix} = \begin{pmatrix} \bar{\boldsymbol{x}} \\ 0 \end{pmatrix} \tag{2.19}$$

for the ith component $(\boldsymbol{x})_i$ of $\boldsymbol{x}$ according to:

$$K_{ij} = U(\boldsymbol{\xi}_i - \boldsymbol{\xi}_j), \quad B_{im} = P_m(\boldsymbol{\xi}_i), \quad \bar{\boldsymbol{\alpha}} = \{(\boldsymbol{\alpha}_m)_i\}_{m=1}^{N+1}, \quad \bar{\boldsymbol{\beta}} = \{(\boldsymbol{\beta}_\ell)_i\}_{\ell=1}^{L}, \quad \bar{\boldsymbol{x}} = \{(\boldsymbol{x}_\ell)_i\}_{\ell=1}^{L}. \tag{2.20}$$

In (2.18) $2!/\alpha!$ is the multinomial coefficient for a multi-index α. While such registrations are easily computed and are often used, the transformation can be pathological enough as to fail to be diffeomorphic [24].

On the other hand, the transformation $\boldsymbol{x}$ has been expressed in terms of *piecewise* polynomial splines and determined by minimizing a weighted sum of the regularity measure (2.18) and the similarity measure (2.12) as seen in [28]. Particularly because of the non-uniqueness of minimizers, the iterative solution of such minimization problems is typically started with the rigid or affine transformation

$$\text{rigid: } \boldsymbol{x}(\boldsymbol{\xi}) = \boldsymbol{\tau} + e^{W}\boldsymbol{\xi}, \quad W = -W^{\mathrm{T}}, \qquad \text{affine: } \boldsymbol{x}(\boldsymbol{\xi}) = \boldsymbol{\tau} + A\boldsymbol{\xi} \tag{2.21}$$

which minimizes the similarity measure.

The kernel of the regularity measure (2.18) selects affine transformations and it thus provides *generalized affine* registration in the sense that an affine transformation is selected when one fits the data. On the other hand, the kernel of (2.18) does not necessarily select a rigid transformation. In order to select rigid transformations it is necessary to consider the full non-linearized elastic potential energy in a regularity measure of the following form [25]:

$$\mathcal{R}_2(\boldsymbol{x}) = \int_{\Omega_0} |\nabla_{\boldsymbol{\xi}}\boldsymbol{x}^{\mathrm{T}}\nabla_{\boldsymbol{\xi}}\boldsymbol{x} - I|^2 d\boldsymbol{\xi} \tag{2.22}$$

However, the corresponding optimality system is quite complex, and *generalized rigid* registration is achieved more easily below with optical flow [20]. A convenient alternative to (2.22) is given by linearized elastic potential energy [6] [26]:

$$\mathcal{R}_3(\boldsymbol{x}) = \mathcal{R}_3(\boldsymbol{d} + I) = \int_{\Omega_0} \left[\lambda[\nabla \cdot \boldsymbol{d}]^2 + \tfrac{1}{2}\mu|\nabla \boldsymbol{d}^T + \nabla \boldsymbol{d}|^2\right] d\boldsymbol{\xi} \tag{2.23}$$

although it does not seleted rigid transformations [20]. A visco-elastic fluid model is adopted with the regularity measure [3] [24]:

$$\mathcal{R}_4(\boldsymbol{x}) = \mathcal{R}_4(\boldsymbol{d} + I) = \int_{\Omega_0} \left[\lambda[\nabla \cdot \boldsymbol{d}_t]^2 + \tfrac{1}{2}\mu|\nabla \boldsymbol{d}_t^T + \nabla \boldsymbol{d}_t|^2\right] d\boldsymbol{\xi} \tag{2.24}$$

where the transformation $\boldsymbol{x}$ is considered to depend upon a time t. In this case, the optimality system for the functional, say, $J(\boldsymbol{x}) = \mathcal{S}_1(\boldsymbol{x}) + \nu\mathcal{R}_4(\boldsymbol{x})$ leads to an evolution equation which may be solved to steady state allowing the regularizing effect of (2.24) to diminish with time.

By using optical flow, generalized affine registration and interpolation is achieved with the regularity measure [17]:

$$\mathcal{R}_5(\boldsymbol{u}) = \int_Q \Big[\sum_{|\alpha|=2} \frac{2!}{\alpha!} |\partial_{\boldsymbol{x}}^{\alpha}\boldsymbol{u}|^2 + \gamma|\boldsymbol{u}_z|^2 \Big] d\boldsymbol{x}dz \tag{2.25}$$

and generalized rigid registration and interpolation is achieved using [20]:

$$\mathcal{R}_6(\boldsymbol{u}) = \int_Q \left[|\nabla_{\boldsymbol{x}}\boldsymbol{u}^{\mathrm{T}} + \nabla_{\boldsymbol{x}}\boldsymbol{u}|^2 + \gamma|\boldsymbol{u}_z|^2\right] d\boldsymbol{x}dz \tag{2.26}$$

While it is shown in [17] that non-autonomous flows are theoretically possible with these regularity measures, a z-dependence is not found in practice. Thus, these integrals over Q can be replaced with integrals over Ω after setting $\gamma = \infty$.

2.4 Optimality Conditions

As an example of image registration by finite displacements, consider the minimization of the following functional:

$$\mathcal{J}_{11}(\boldsymbol{x}) = \mathcal{S}_1(\boldsymbol{x}) + \nu\mathcal{R}_1(\boldsymbol{x}). \tag{2.27}$$

This functional is stationary when $\boldsymbol{x}$ satisfies:

$$0 = \frac{1}{2}\frac{\delta\mathcal{J}_{11}}{\delta\boldsymbol{x}}(\boldsymbol{x},\bar{\boldsymbol{x}}) = \mathcal{B}_{11}(\boldsymbol{x},\bar{\boldsymbol{x}}) - \mathcal{F}_{11}(\boldsymbol{x},\bar{\boldsymbol{x}}), \quad \forall\bar{x}\in H^2(\Omega,\boldsymbol{R}^N) \tag{2.28}$$

where $H^m(\Omega,\boldsymbol{R}^N)$ is the Sobolev space of functions mapping Ω into $\boldsymbol{R}^N$ with Lebesgue square integrable derivatives up to order m, and $\mathcal{B}_{11}$ and $\mathcal{F}_{11}$ are defined by [17]:

$$\mathcal{B}_{11}(\boldsymbol{x},\bar{\boldsymbol{x}}) = \nu\sum_{|\alpha|=2}\frac{2!}{\alpha!}\int_{\Omega_0}[\partial^\alpha_{\boldsymbol{\xi}}\boldsymbol{x}]\cdot[\partial^\alpha_{\boldsymbol{\xi}}\bar{\boldsymbol{x}}]d\boldsymbol{\xi} \tag{2.29}$$

$$\mathcal{F}_{11}(\boldsymbol{x},\bar{\boldsymbol{x}}) = \int_{\Omega_0}\left[I_0(\boldsymbol{\xi}) - I_1(\boldsymbol{x}(\boldsymbol{\xi}))\right]\nabla_{\boldsymbol{x}}I_1(\boldsymbol{x}(\boldsymbol{\xi}))^{\mathrm{T}}\bar{\boldsymbol{x}}(\boldsymbol{\xi})d\boldsymbol{\xi}. \tag{2.30}$$

The form $\mathcal{F}_{11}$ contains a similar term over Ω_1 when $\mathcal{S}_1$ contains the corresponding term mentioned in relation to (2.5). The transformation $\boldsymbol{x}$ satisfying (2.28) can be computed by the following quasi-Newton iteration [17]:

$$\left\{\begin{array}{rcl}\mathcal{N}_{11}(\boldsymbol{dx}_k,\boldsymbol{x}_k,\bar{\boldsymbol{x}}) &=& -\left[\mathcal{B}_{11}(\boldsymbol{x}_k,\bar{\boldsymbol{x}}) - \mathcal{F}_{11}(\boldsymbol{x}_k,\bar{\boldsymbol{x}})\right], \quad \forall\bar{\boldsymbol{x}}\in H^2(\Omega_0,\boldsymbol{R}^N)\\ \boldsymbol{x}_{k+1} &=& \boldsymbol{x}_k + \theta\boldsymbol{dx}_k\end{array}\right. \qquad k=0,1,2,\ldots \tag{2.31}$$

where:

$$\mathcal{N}_{11}(\boldsymbol{dx}_k,\boldsymbol{x}_k,\bar{\boldsymbol{x}}) = \mathcal{B}_{11}(\boldsymbol{dx}_k,\bar{\boldsymbol{x}}) + \int_{\Omega_0}[\nabla_{\boldsymbol{x}}I_1(\boldsymbol{x}_k(\boldsymbol{\xi}))\cdot\boldsymbol{dx}_k(\boldsymbol{\xi})][\nabla_{\boldsymbol{x}}I_1(\boldsymbol{x}_k(\boldsymbol{\xi}))\cdot\bar{\boldsymbol{x}}(\boldsymbol{\xi})]d\boldsymbol{\xi} \tag{2.32}$$

and θ is chosen by a line search to minimize $\mathcal{S}_1$ [12]. Note that no additional boundary conditions are imposed by restricting the domain of the forms defined above, and thus natural boundary conditions hold.

As an example of image registration and interpolation by optical flow, consider the minimization of the following functional:

$$\mathcal{J}_{26}(\boldsymbol{u},I) = \mathcal{S}_2(\boldsymbol{u},I) + \nu\mathcal{R}_6(\boldsymbol{u}). \tag{2.33}$$

This functional is stationary in the optical flow $\boldsymbol{u}$ for fixed I when $\boldsymbol{u}$ satisfies:

$$0 = \frac{1}{2}\frac{\delta\mathcal{J}_{26}}{\delta\boldsymbol{u}}(\boldsymbol{u},\bar{\boldsymbol{u}}) = \mathcal{B}_{26}(\boldsymbol{u},\bar{\boldsymbol{u}}) - \mathcal{F}_{26}(\bar{\boldsymbol{u}}), \quad \forall\bar{\boldsymbol{u}}\in H^1(Q,\boldsymbol{R}^N), \tag{2.34}$$

where $\mathcal{B}_{26}$ and $\mathcal{F}_{26}$ are defined by [20]:

$$\begin{aligned}\mathcal{B}_{26}(\boldsymbol{u},\bar{\boldsymbol{u}}) &= \int_Q\left[(\nabla I\cdot\boldsymbol{u})(\nabla I\cdot\bar{\boldsymbol{u}}) + \gamma\left(\boldsymbol{u}_z\cdot\bar{\boldsymbol{u}}_z\right)\right]d\boldsymbol{x}dz\\ &+ \int_Q\tfrac{1}{2}\left(\nabla\boldsymbol{u}^{\mathrm{T}} + \nabla\boldsymbol{u}\right) : \left(\nabla\bar{\boldsymbol{u}}^{\mathrm{T}} + \nabla\bar{\boldsymbol{u}}\right)d\boldsymbol{x}dz\end{aligned} \tag{2.35}$$

$$\mathcal{F}_{26}(\bar{\boldsymbol{u}}) = -\int_Q I_z\nabla I\cdot\bar{\boldsymbol{u}}d\boldsymbol{x}dz. \tag{2.36}$$

Note that no additional boundary conditions are imposed by restricting the domain of these forms, and thus natural boundary conditions hold.

The optimality condition for $\mathcal{J}_{26}$ with respect to the intensity I involves to solve the equation $d^2I/d\zeta^2 + (\nabla \cdot \boldsymbol{u})dI/d\zeta = 0$ with boundary conditions as seen in Fig. 2. When this condition is formulated and solved in an Eulerian fashion, the resulting interpolated images lose clarity between Ω_0 and Ω_1 [20]. Thus, the optimality condition on the intensity should be formulated in a Lagrangian fashion. Specifically, the functional $\mathcal{J}_{26}$ is stationary in the intensity I for fixed $\boldsymbol{u}$ when I satisfies the following in terms of quantities defined below [20]:

$$I(\boldsymbol{x}(\boldsymbol{\xi},\zeta),\zeta) = \begin{cases} I_0(\boldsymbol{\xi})[1-U(\boldsymbol{\xi},\zeta,1)] + I_1(\boldsymbol{x}(\boldsymbol{\xi},1))U(\boldsymbol{\xi},\zeta,1), & \boldsymbol{\xi}\in\Omega_0^{\mathrm{c}} \\ I_0(\boldsymbol{\xi})[1-U(\boldsymbol{\xi},\zeta,\acute{\zeta})], & \boldsymbol{x}(\boldsymbol{\xi},\acute{\zeta})\in\Gamma,\ \boldsymbol{\xi}\in\Omega_0^{\mathrm{i}} \end{cases} \tag{2.37}$$

$$I(\boldsymbol{y}(\boldsymbol{\eta},\zeta),\zeta) = \begin{cases} I_1(\boldsymbol{\eta})[1-V(\boldsymbol{\eta},0,\zeta)] + I_0(\boldsymbol{y}(\boldsymbol{\eta},0))V(\boldsymbol{\eta},0,\zeta), & \boldsymbol{\eta}\in\Omega_1^{\mathrm{c}} \\ I_1(\boldsymbol{\eta})[1-V(\boldsymbol{\eta},\grave{\zeta},\zeta)], & \boldsymbol{y}(\boldsymbol{\eta},\grave{\zeta})\in\Gamma,\ \boldsymbol{\eta}\in\Omega_1^{\mathrm{i}}. \end{cases} \tag{2.38}$$

As illustrated in Fig. 2, the parameters $\acute{\zeta}$ and $\grave{\zeta}$ denote the ζ coordinates at which trajectories emanating respectively from Ω_0^{i} and Ω_1^{i} meet Γ. Then, U and V are defined by:

$$U(\boldsymbol{\xi},\zeta,\acute{\zeta}) = \frac{\tilde{U}(\boldsymbol{\xi},\zeta)-\tilde{U}(\boldsymbol{\xi},0)}{\tilde{U}(\boldsymbol{\xi},\acute{\zeta})-\tilde{U}(\boldsymbol{\xi},0)}, \qquad \tilde{U}(\boldsymbol{\xi},\zeta) = \int_{\zeta_0}^{\zeta} \exp\left[-\int_{\zeta_0}^{\varrho} \nabla\cdot\boldsymbol{u}(\boldsymbol{x}(\boldsymbol{\xi},\rho),\rho)d\rho\right] d\varrho, \tag{2.39}$$

for $\boldsymbol{\xi}\in\Omega_0$, $\zeta\in[0,\acute{\zeta}]$, and arbitrary $\zeta_0\in[0,\acute{\zeta}]$, and:

$$V(\boldsymbol{\eta},\grave{\zeta},\zeta) = \frac{\tilde{V}(\boldsymbol{\eta},1)-\tilde{V}(\boldsymbol{\eta},\zeta)}{\tilde{V}(\boldsymbol{\eta},1)-\tilde{V}(\boldsymbol{\eta},\grave{\zeta})}, \qquad \tilde{V}(\boldsymbol{\eta},\zeta) = \int_{\zeta_0}^{\zeta} \exp\left[-\int_{\zeta_0}^{\varrho} \nabla\cdot\boldsymbol{u}(\boldsymbol{y}(\boldsymbol{\eta},\rho),\rho)d\rho\right] d\varrho, \tag{2.40}$$

for $\boldsymbol{\eta}\in\Omega_1$, $\zeta\in[\grave{\zeta},1]$, and arbitrary $\zeta_0\in[\grave{\zeta},1]$. These formulas can be easily interpreted by considering the case that the transformation is rigid and thus $\nabla\cdot\boldsymbol{u}=0$ holds. In this case, I must satisfy $d^2I/d\zeta^2=0$ and $U(\boldsymbol{\xi},\zeta,1)=\zeta$ and $V(\boldsymbol{\eta},0,\zeta)=(1-\zeta)$ hold.

If the similarity measure $\mathcal{S}_2$ of $\mathcal{J}_{26}$ is modified to incorporate intensity scaling as seen in (2.10), then under the simplifying assumption that the given images are piecewise constant the functional $\mathcal{J}_{26}$ is stationary in the scaling function σ_0 for fixed optical flow $\boldsymbol{u}$ and intensity I when σ_0 satisfies [16]:

$$\sigma_0(\iota) = \int_{I_0(\boldsymbol{\xi})=\iota} \mathcal{I}_1(\boldsymbol{\xi})\mathcal{U}(\boldsymbol{\xi})d\boldsymbol{\xi} \Big/ \int_{I_0(\boldsymbol{\xi})=\iota} \mathcal{U}(\boldsymbol{\xi})d\boldsymbol{\xi} \tag{2.41}$$

where the morphing of I_1 into Ω_0 is given by:

$$\mathcal{I}_1(\boldsymbol{\xi}) = \begin{cases} I_1(\boldsymbol{x}(\boldsymbol{\xi},1)), & \boldsymbol{\xi}\in\Omega_0^{\mathrm{c}} \\ 0, & \boldsymbol{\xi}\in\Omega_0^{\mathrm{i}} \end{cases} \tag{2.42}$$

and $\mathcal{U}$ is defined by:

$$\mathcal{U}(\boldsymbol{\xi}) = \begin{cases} \displaystyle\int_0^1 U_\zeta^2(\boldsymbol{\xi},\zeta,1)\det\left(\nabla_{\boldsymbol{\xi}}\boldsymbol{x}\right)d\zeta, & \boldsymbol{\xi}\in\Omega_0^{\mathrm{c}} \\ \displaystyle\int_0^{\acute{\zeta}(\boldsymbol{\xi})} U_\zeta^2(\boldsymbol{\xi},\zeta,\acute{\zeta}(\boldsymbol{\xi}))\det\left(\nabla_{\boldsymbol{\xi}}\boldsymbol{x}\right)d\zeta, & \boldsymbol{\xi}\in\Omega_0^{\mathrm{i}} \end{cases} \tag{2.43}$$

These formulas can be easily interpreted by considering the case that the transformation is rigid. It follows from $\nabla\cdot\boldsymbol{u}=0$ that $U(\boldsymbol{\xi},\zeta,1)=\zeta$, $U_\zeta(\boldsymbol{\xi},\zeta,1)=1$ and $\det(\nabla_{\boldsymbol{\xi}}\boldsymbol{x})=1$ hold. Thus, $\mathcal{U}(\boldsymbol{\xi})=1$ holds. The formula (2.41) determines the value of $\sigma_0(\iota)$ as the average value of morphed image over the level set $I_0(\boldsymbol{\xi})=\iota$. When the transformation is not rigid, the value of $\sigma_0(\iota)$ is a weighted average of the morphed image over the level set.

To incorporate the landmark constraints (2.15) into the determination of finite displacements, $\mathcal{J}_{11}$ for instance may be augmented to form the following Lagrangian functional [26] [7]:

$$\mathcal{L}_{11}(\boldsymbol{x}, \boldsymbol{\lambda}) = \tfrac{1}{2}\mathcal{J}_{11}(\boldsymbol{x}) + \sum_{\ell=1}^{L} \boldsymbol{\lambda}_\ell^{\mathrm{T}} \boldsymbol{\mathcal{E}}_\ell(\boldsymbol{x}). \tag{2.44}$$

This Lagrangian functional is stationary in $(\boldsymbol{x}, \boldsymbol{\lambda}_1, \ldots, \boldsymbol{\lambda}_L)$ when the following hold:

$$\left\{ \begin{array}{rcl} \mathcal{B}_{11}(\boldsymbol{x}, \bar{\boldsymbol{x}}) - \mathcal{F}_{11}(\boldsymbol{x}, \bar{\boldsymbol{x}}) + \displaystyle\sum_{\ell=1}^{L} \boldsymbol{\lambda}^{\mathrm{T}} \bar{\boldsymbol{x}}(\boldsymbol{\xi}_\ell) & = & 0, \quad \forall \bar{\boldsymbol{x}} \in H^2(\Omega, \boldsymbol{R}^N), \\ \\ \boldsymbol{x}(\boldsymbol{\xi}_\ell) - \boldsymbol{x}_\ell & = & 0, \quad \ell = 1, \ldots, L. \end{array} \right. \tag{2.45}$$

For this, let $U_\ell(\boldsymbol{\xi}) = U(\boldsymbol{\xi} - \boldsymbol{\xi}_\ell)$ be the solution to $\mathcal{B}_{11}(U_\ell, \bar{U}) + \bar{U}(\boldsymbol{\xi}_\ell) = 0$, $\forall \bar{U} \in H^2(\Omega, \boldsymbol{R})$; cf. (2.17). Also, let $\tilde{\boldsymbol{x}}$ be the solution to $\mathcal{B}_{11}(\tilde{\boldsymbol{x}}, \bar{\boldsymbol{x}}) - \mathcal{F}_{11}(\boldsymbol{x}, \bar{\boldsymbol{x}}) = 0$, $\forall \bar{\boldsymbol{x}} \in H^2(\Omega, \boldsymbol{R}^N)$. Then determine the Lagrange multipliers $\{\boldsymbol{\lambda}_\ell\}$ algebraically from the condition that $\boldsymbol{x} = \tilde{\boldsymbol{x}} + \sum_{\ell=1}^{L} \boldsymbol{\lambda}_\ell U_\ell(\boldsymbol{\xi})$ satisfy the landmark constraints (2.15). Thus, $(\boldsymbol{x}, \boldsymbol{\lambda}_1, \ldots, \boldsymbol{\lambda}_L)$ satisfy (2.45). Of course, $\tilde{\boldsymbol{x}}$ and $\boldsymbol{x}$ depend upon each other, and these may be computed iteratively. Note that the formulation of landmark constraints for optical flow is more complicated [18].

2.5 Processing Image Sequences

An image sequence may be registered or interpolated of course by processing the images only pairwise and concatenating the results. On the other hand, a coupling among images may be introduced as follows; see also [24].

The images of a sequence $\{I_k\}_{l=0}^{K}$ can be registered simultaneously using finite displacements $\{\boldsymbol{x}_k\}_{l=1}^{K}$ by minimizing:

$$\mathcal{J}_{11}^{(K)}(\boldsymbol{x}_1, \ldots, \boldsymbol{x}_K) = \sum_{k=1}^{K} \mathcal{S}_1^{(k)}(\boldsymbol{x}_1, \ldots, \boldsymbol{x}_K) + \mathcal{R}_1(\boldsymbol{x}_l) \tag{2.46}$$

where:

$$\mathcal{S}_1^{(k)}(\boldsymbol{x}_1, \ldots, \boldsymbol{x}_K) = \sum_{|l-j|=1} \int_{\Omega_k} \left[I_j(\boldsymbol{x}_j(\boldsymbol{\xi})) - I_l(\boldsymbol{x}_l(\boldsymbol{\xi})) \right]^2 d\boldsymbol{\xi} \tag{2.47}$$

where all images are extended by their background intensities (here as before assumed to be zero) outside their domains, Ω_l, which are additional counterparts to Ω_0 and Ω_1 depicted in Fig. 1. The end indices $k = 0$ and $k = K$ in (2.46) correspond to pairwise registration with the single near neighbor. When (2.46) has been minimized, the point $\boldsymbol{x}_i(\boldsymbol{\xi}) \in \Omega_i$ has been matched to the point $\boldsymbol{x}_j(\boldsymbol{\xi}) \in \Omega_j$. To minimize ${\mathcal{J}_{11}}^{(K)}$ with respect to $\boldsymbol{x}_k$ while all other transformations are held fixed, replace $\mathcal{F}_{11}$ in (2.28) and (2.31) with ${\mathcal{F}_{11}}^{(k)} = -\frac{1}{2}\delta {\mathcal{S}_1}^{(k)}/\delta \boldsymbol{x}$:

$$\mathcal{F}_{11}^{(k)}(\boldsymbol{x}_k, \bar{\boldsymbol{x}}) = \int_{\Omega_k} \sum_{|k-j|=1} \left[I_j(\boldsymbol{x}_j(\boldsymbol{\xi})) - I_k(\boldsymbol{x}_k(\boldsymbol{\xi})) \right] \nabla_{\boldsymbol{x}} I_k(\boldsymbol{x}_k(\boldsymbol{\xi}))^{\mathrm{T}} \bar{\boldsymbol{x}}(\boldsymbol{\xi}) d\boldsymbol{\xi}. \tag{2.48}$$

The functional of (2.46) can be minimized by freezing all current transformations except for one, minimizing the functional with respect to the selected transformation, updating that transformation immediately (Gauss-Seidel strategy) or else updating all transformations simultaneously (Jacobi strategy), and then repeating the process until the updates have converged. Known transformations can remain frozen as fixed boundary conditions, e.g., at one or both of the end indices $k = 0$ and $k = K$ in (2.46) when the position of one or both of the end images I_0 and I_K is known.

The calculation (2.48) shows that $\mathcal{J}_{11}^{(L)}$ is just as well minimized with respect to $\boldsymbol{x}_k$ by registering the image I_k with the image $I_{k_{\mathrm{n}}}(\boldsymbol{\xi}) = \sum_{|j-k|=1} I_j(\boldsymbol{x}_j(\boldsymbol{\xi})) / \sum_{|j-k|=1} 1$. Analogously,

the images $\{I_k\}_{k=0}^K$ can be registered simultaneously by computing autonomous optical flows $\{\boldsymbol{u}_k\}_{k=0}^K$ for the image pairs $\{[I_k, I_{k_n}]\}_{k=0}^K$ according to pairwise procedures, where the transformations $\{\boldsymbol{x}_k\}_{k=0}^K$ are computed by using their respective flows in (2.4). Then the flows and their corresponding transformations can be updated repeatedly until convergence, where known transformations can remain frozen as fixed boundary conditions as discussed above.

The images $\{I_k\}_{k=0}^K$ can be interpolated from autonomous optical flows $\{\boldsymbol{u}_k\}_{k=0}^{K-1+M}$ using the semi-discretization defined on $Q^{(K)} = \Omega \times (0, K)$:

$$\boldsymbol{u}(\boldsymbol{x}, z) = \sum_{k=0}^{K} \boldsymbol{u}_k(\boldsymbol{x}) \chi_k^M(z) \tag{2.49}$$

where $\{\chi_k^M\}_{k=0}^{K-1+M}$ is a basis for the canonical B-splines of degree M defined on the grid $\{[k, k+1]\}_{k=0}^{K-1}$ of $[0, K]$ [14]. Then the transformations are given by natural modifications of (2.4) replacing Ω_0, Ω_1 and $\zeta \in [0, 1]$ with Ω_k, Ω_{k+1} and $\zeta \in [k, k+1]$. Also, the intensity I is given by natural modifications of (2.37) and (2.38) replacing Ω_0, Ω_1 and Γ with Ω_k, Ω_{k+1} and $\Gamma^{(K)} = \partial Q^{(K)} \backslash \{\Omega_0 \cup \Omega_K\}$. For instance, for $M = 0$, χ_k^0 is the characteristic function for the interval $[k, k+1]$, and the above procedure corresponds to pairwise interpolation of the given images. When smoother trajectories and greater coupling among images are desired, higher order splines can be used in (2.49), and (2.34) can be solved for $\{\boldsymbol{u}_k\}_{k=0}^{K-1+M}$ with $\gamma = 0$ and Q replaced by $Q^{(K)}$.

2.6 Numerical Methods

The most costly computations required to solve the optimality systems of the previous subsection are those involved with the solution to (2.28) and (2.34). It is shown in [20] that the trajectory integrations must be performed from every point in Q where the intensity I is needed, and trajectories must be extended in both directions toward Ω_0 and Ω_1 in order to connect values of I_0 and I_1; nevertheless, such integrations can be vectorized and obtained remarkably quickly. All other computations are even less expensive in relation to those required for (2.28) and (2.34).

For the numerical solution of the finite displacement problem (2.28) or of the (autonomous) optical flow problem (2.34), it is useful to consider the common structure among such problems, which is found often in image processing. Specifically, the boundary value problems have the form:

$$\begin{aligned}&\text{Find } \boldsymbol{\varphi} \in H^\kappa(\Omega, \boldsymbol{R}^N) \text{ such that:}\\ &\nu(\mathcal{D}^{(\kappa)}\boldsymbol{\varphi}, \mathcal{D}^{(\kappa)}\boldsymbol{\psi})_{L^2(\Omega,\boldsymbol{R}^N)} + (\boldsymbol{g}\cdot\boldsymbol{\varphi}, \boldsymbol{g}\cdot\boldsymbol{\psi})_{L^2(\Omega,\boldsymbol{R}^N)} = (\boldsymbol{f}, \boldsymbol{\psi})_{L^2(\Omega,\boldsymbol{R}^N)}, \quad \text{for all } \boldsymbol{\psi} \in H^\kappa(\Omega, \boldsymbol{R}^N)\end{aligned} \tag{2.50}$$

where $\boldsymbol{g} \in L^\infty(\Omega, \boldsymbol{R}^N)$ and $\boldsymbol{f} \in L^2(\Omega, \boldsymbol{R}^N)$ have the same compact support in Ω, and $\mathcal{D}^{(\kappa)}$ is a differential operator of order κ. The $\mathcal{D}^{(\kappa)}$-regularization term as well as the $\boldsymbol{g}$-data term are both indefinite on $H^\kappa(\Omega, \boldsymbol{R}^N)$, but the sum is bounded and coercive. With additional homogeneous boundary conditions, the $\mathcal{D}^{(\kappa)}$-regularization term can be made definite and therefore numerically better conditioned, but such artificial boundary conditions would corrupt a generalized rigid or generalized affine approach. While Fourier methods have been used for similar systems [6] [24], multigrid methods [12] [13] [17] can be used with comparable speed and greater generality, for instance, to accommodate the natural boundary conditions associated with (2.50).

A geometric multigrid formulation is developed in [17] for (2.28) and (2.34) and is based upon [10]. The usual multigrid strategy is generally to enhance a convergent relaxation scheme by using its initial and rapid smoothing of small scales on finer grids and then to transfer the problem progressively to coarser grids before relaxation is decelerated. The principal ingredients of the strategy include the definition of a smoothing relaxation scheme and the definition of a coarse grid representation of the problem which can be used to provide an improvement or correction on a finer grid.

For the representation of the boundary value problem on progressively coarser grids, (2.50) can be formulated on a nested sequence of finite element subspaces $S^\kappa_{2h}(\Omega, \boldsymbol{R}^N) \subset S^\kappa_h(\Omega, \boldsymbol{R}^N)$ such as tensor products of the B-splines illustrated in Fig. 3. Then the finite element approxi-

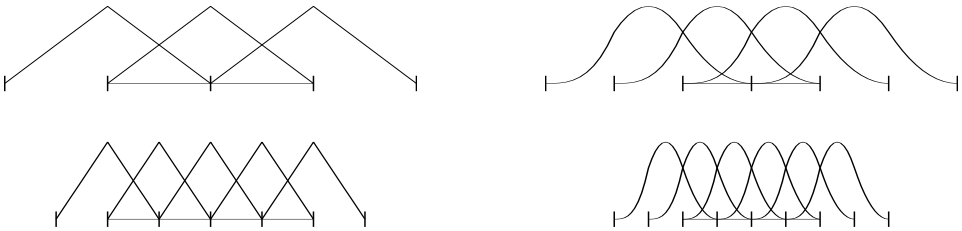

Figure 3: Examples of nested finite elements spaces $S^\kappa_{2h}(\Omega, \boldsymbol{R}^1) \subset S^\kappa_h(\Omega, \boldsymbol{R}^1)$ of degree 1 (left column) and 2 (right column).

mation to the solution $\boldsymbol{\varphi}$ of (2.50) is $\boldsymbol{\varphi}_h \in S^\kappa_h(\Omega, \boldsymbol{R}^N)$ defined by replacing $H^\kappa(\Omega, \boldsymbol{R}^N)$ in (2.50) with $S^\kappa_h(\Omega, \boldsymbol{R}^N)$. This finite-dimensional formulation is expressed as $A_h\Phi_h = F_h$ where A_h is the matrix representation of the differential operator in the finite element basis and Φ_h and F_h are vectors of finite element basis coefficients for $\boldsymbol{\varphi}_h$ and $\boldsymbol{f}$ respectively. Let K_h denote the mapping from coefficients to functions so that $\Phi_h = K_h\boldsymbol{\varphi}_h$ holds. Also, let I_{2h} denote the injection operator from $S^\kappa_{2h}(\Omega, \boldsymbol{R}^N)$ into $S^\kappa_h(\Omega, \boldsymbol{R}^N)$. Then the coarse grid matrix A_{2h} is computed from the fine grid matrix A_h according to the Galerkin approximation $A_{2h} = R^{2h}_h A_h E^h_{2h}$ where E^h_{2h} and R^{2h}_h are the canonical expansion and restriction operators satisfying $I_{2h}K_{2h} = K_h E^h_{2h}$ and $(E^h_{2h})^* = R^{2h}_h$. In words, E^h_{2h} produces *coefficients* $\boldsymbol{\Phi}_h = E^h_{2h}\boldsymbol{\Phi}_{2h}$ from coefficients $\boldsymbol{\Phi}_{2h}$ so that the *function* $K_h\boldsymbol{\Phi}_h$ is identical to the function $K_{2h}\boldsymbol{\Phi}_{2h}$. With the coarse grid problem and the intergrid transfer operators defined, it remains to identify a suitable relaxation scheme and to define the multigrid iteration.

Since the bilinear form in (2.50) is symmetric and coercive, the matrices, $A_h = \mathcal{D}_h + \mathcal{L}_h + \mathcal{L}^{\mathrm{T}}_h$, are symmetric and positive definite, where $\mathcal{D}_h$ is strictly diagonal and $\mathcal{L}_h$ is strictly lower triangular. Thus, it is natural to use a symmetric relaxation scheme such as the symmetric successive over-relaxation,

$$\boldsymbol{\Phi}^{k+1}_h = S_h\boldsymbol{\Phi}^k_h + \omega W^{-1}_h F_h, \qquad S_h = I - \omega W^{-1}_h A_h, \quad W_h = (\mathcal{D}_h + \mathcal{L}_h)\mathcal{D}^{-1}_h(\mathcal{D}_h + \mathcal{L}^{\mathrm{T}}_h), \quad \omega \in (0, 2). \tag{2.51}$$

As discussed in detail in [19], this relaxation scheme can be vectorized for implementation in systems such as IDL or MATLAB by using a multi-colored ordering of cells as illustrated in Fig. 4 for a stencil diameter of 3 cells. In general, for a stencil diameter of $(2\kappa + 1)$, define a set of *same-color* cells as those which are separated from one another in any of N coordinate directions by exactly κ cells. These cells have stencils which do not weight any other cells in the set; thus, the strategy is to update such sets of cells simultaneously in the relaxation. Such same-color cells are ordered along coordinate directions within that color, and then ordered sequentially among the colors. With such a multi-colored ordering, the relaxation scheme can be implemented by performing a Jacobi iteration on same-colored cells while looping in one direction and then the other over the colors.

$$\text{for } c = 1, \ldots, (\kappa+1)^N \text{ and then } c = (\kappa+1)^N, \ldots, 1 \text{ do: } \Phi^{\mathrm{c}}_h \leftarrow \Phi^{\mathrm{c}}_h - [\mathcal{D}^{-1}_h(A_h\Phi_h - F_h)]^{\mathrm{c}} \tag{2.52}$$

In this way, same-colored cells are updated simultaneously. Similarly, the known stencil diameter can also be used to advantage to vectorize the computation of elements of the coarse grid matrix [19].

With the above ingredients, a symmetric two-grid cycle $\mathrm{TGC}(h, \sigma)$ is obtained by:

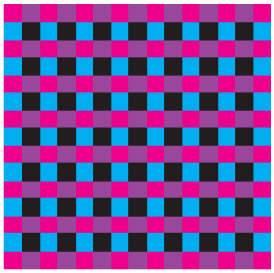

Figure 4: A multi-color ordering of cells for a stencil diameter of $2\kappa + 1(= 3)$ in which same-color cells are separated from one another in any of $N(= 2)$ coordinate directions by exactly $\kappa(= 1)$ cells.

1) performing σ relaxation steps to update Φ_h,
2) computing the coarse-grid residual $D_{2h} = R^h_{2h}(F - A_h\Phi_h)$,
3) solving on the coarse grid $A_{2h}\Psi_{2h} = D_{2h}$,
4) correcting on the fine grid $\Phi_h \leftarrow \Phi_h + E^h_{2h}\Psi_{2h}$, and finally
5) performing another σ relaxation steps to update Φ_h.

Then a symmetric multigrid cycle $\mathrm{MGC}(h, \sigma, \tau)$ is defined as with the two-grid cycle except that step (3) in $\mathrm{TGC}(h, \sigma)$ is recursively replaced with τ iterations of $\mathrm{MGC}(2h, \sigma, \tau)$ unless $2h$ is large enough that the the coarse grid problem may easily be solved exactly.

2.7 Computational Examples

Here examples of generalized affine and generalized rigid image registration and interpolation are shown together with examples of intensity scaling. Shown in Fig. 5 are two given images

a) Images on the far left and right are registered and interpolated by minimizing $\mathcal{S}_2 + \nu\mathcal{R}_5$.

b) images on the far left and right are registered and interpolated by minimizing $\mathcal{S}_2 + \nu\mathcal{R}_6$.

Figure 5: For the images shown on the far left and right, which may related by either an affine or by a rigid transformation, the results of minimiziing $\mathcal{S}_2 + \nu\mathcal{R}_5$ and $\mathcal{S}_2 + \nu\mathcal{R}_6$ are shown respectively in the first and second rows.

on the far left and on the far right, which may be related by either an affine or by a rigid transformation. The results of minimizing $\mathcal{S}_2 + \nu\mathcal{R}_5$ and $\mathcal{S}_2 + \nu\mathcal{R}_6$ to register and to interpolate between the given images are shown respectively in the top and bottom rows. The figure shows that $\mathcal{R}_5$ and $\mathcal{R}_6$ produce affine and rigid transformations respectively when such transformations fit the data.

For the case that the given data are not related by such a simple transformation, e.g., by a rigid transformation, Fig. 6 shows that the departure from rigidity may be controlled by the regularization parameter ν. Specifically, the result for larger ν is strongly rigid while the result for smaller ν is called weakly rigid [20]. Also, strong or weak rigidity may be controlled locally by incorporating ν into the regularization penalty $\mathcal{R}_6$ as a distributed parameter; see [25].

Finally, the intensity scaling approach of (2.10) and (2.41) is illustrated in Fig. 7. Let the upper image sequence here be denoted by $I^{(0)}(t)$, $0 \le t \le 1$, and the middle image sequence

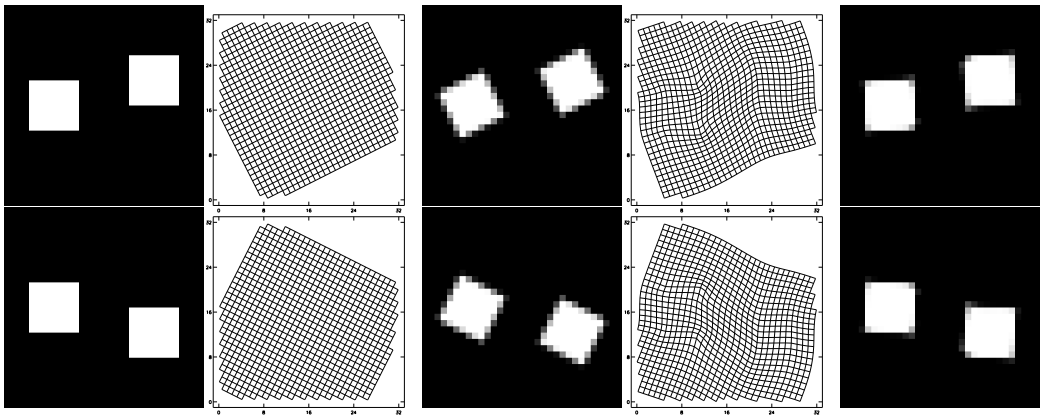

Figure 6: The given images are shown in the far left column. These images are registered by minimizing $\mathcal{S}_2 + \nu\mathcal{R}_6$, and the results for large ν are shown in the second and third rows while the results for smaller ν are shown in the fourth and fifth rows. In each case, registration results are illustrated by applying the transformation, as well as its inverse, first to a uniform grid and then to the given image situated on the front or on the back face of Q in Fig. 1.

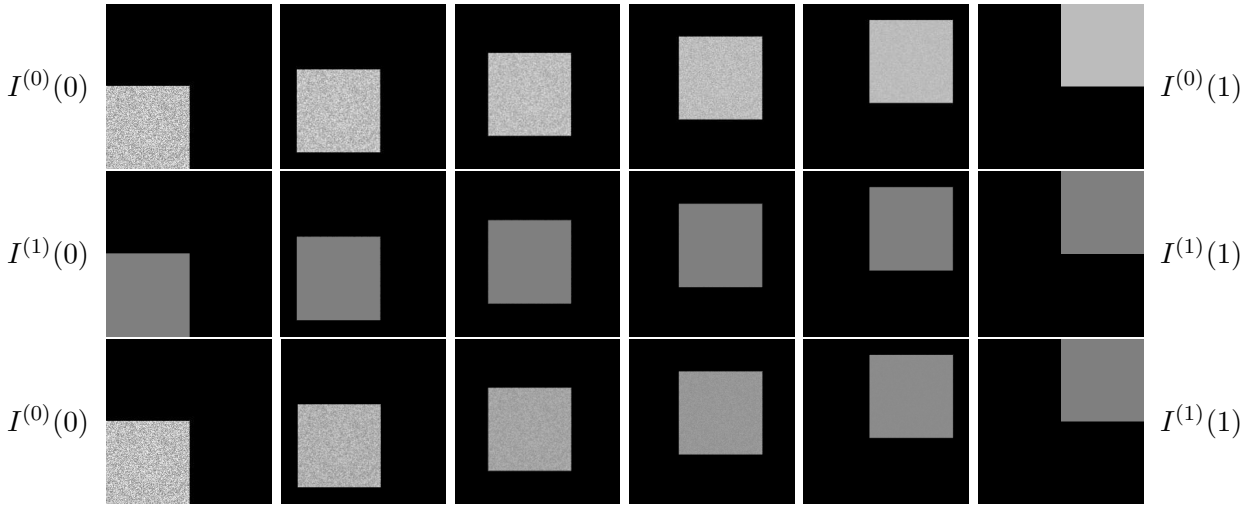

Figure 7: The image sequences, $I^{(0)}(t)$ and $I^{(1)}(t)$, $t = 0, .2, .4, .6, .8, 1$, are shown in the top two rows. The given raw images are at the upper left $I^{(0)}(0)$ and at the middle right $I^{(1)}(1)$. The intensity scaling of (2.10) and (2.41) transforms the upper left $I^{(0)}(0)$ into the middle left image $I^{(1)}(0)$ and the middle right $I^{(1)}(1)$ into the upper right image $I^{(0)}(1)$. Registration and interpolation are then performed independently in the top two rows by minimizing $\mathcal{S}_2 + \nu\mathcal{R}_6$. The convex convex combination $(t-1)I^{(0)}(t) + tI^{(1)}(t)$ of these sequences gives the interpolation shown in the third row.

by $I^{(1)}(t)$, $0 \le t \le 1$, where the given raw images are at the upper left $I^{(0)}(0)$ and at the middle right $I^{(1)}(1)$. These two images have different histograms and different noise levels, but the intensity scaling of (2.10) and (2.41) transforms the upper left $I^{(0)}(0)$ into the middle left image $I^{(1)}(0)$ and the middle right $I^{(1)}(1)$ into the upper right image $I^{(0)}(1)$. Once the images are rescaled in this way, registration and interpolation may be performed independently in the top two rows by minimizing $\mathcal{S}_2 + \nu\mathcal{R}_6$. The interpolation between the given images is then given by the convex combination $(t-1)I^{(0)}(t) + tI^{(1)}(t)$ as shown in the third row of Fig. 7. This is precisely the procedure used to interpolate between the raw magnetic resonance images shown on the left and on the right in Fig. 8. These raw images have been measured in the course of respiration and they have different histograms because of the appearance of contrast agent [16] [17]. The two raw images shown in Fig. 8 are part of the larger sequence `http://math.uni-graz.at/keeling/respfilm1.mpg` which is interpolated as seen in `http://math.uni-graz.at/keeling/respfilm2.mpg`.

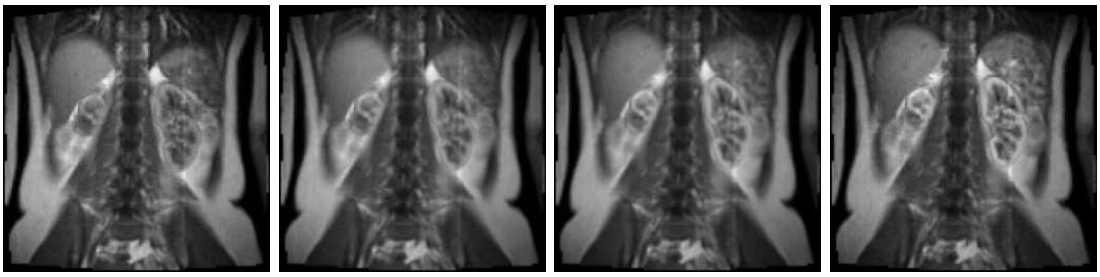

Figure 8: Shown on the left and on the right are two given raw magnetic resonance images measured in the course of respiration and the introduction of contrast agent. The images in between have been interpolated by minimizing $\mathcal{S}_2 + \nu\mathcal{R}_6$ using the scaling approach of (2.10) and (2.41).

References

[1] R.A. Adams, *Sobolev Spaces*, Academic Press, New York, 1975.

[2] V. Caselles and L. Garrido, *A contrast invariant approach to motion estimation*, Scale Space 2005, Hofgeismar, Germany, 7-9 April, 2005.

[3] G.E. Christensen, *Deformable Shape Models for Anatomy*, Ph.D. Thesis, Sever Institute of Technology, Washington University, 1994.

[4] M. Droske and M. Rumpf, *A Variational Approach to Non-Rigid Morphological Registration*, SIAM J. Appl. Math., Vol. 64, No. 2, pp. 668–687, 2004.

[5] M. Droske and W. Ring, *A Mumford-Shah Level-Set Approach for Geometric Image Registration*, Preprint Series DFB-SPP 1114, Preprint 99, April 2005.

[6] B. Fischer and J. Modersitzki, *Fast Inversion of Matrices Arising in Image Processing*, Numerical Algorithms 22, pp. 1–11, 1999.

[7] B. Fischer and J. Modersitzki, *Combination of automatic non-rigid and landmark based registration: the best of both worlds*, Medical Imaging 2003: Image Processing, M. Sonka, J.M. Fitzpatrick (eds.), Proceedings of the SPIE 5032, pp. 1037–1048, 2003.

[8] M. Fitzpatrick, D.L.G. Hill and C.R. Maurer, Jr., *Image Registration*, Medical Image Processing, Chapter 8 of Volume II of the Handbook of Medical Imaging, M. Sonka and J.M. Fitzpatrick, ed., SPIE Press (July, 2000).

[9] M. Fitzpatrick, J.B. West, and C.R. Maurer, Jr., *Predicting Error in Rigid-Body Point-Based Registration*, IEEE Trans. Med. Imaging, Vol. 17, pp. 694–702, 1998.

[10] W. Hackbusch, *Iterative Solution of Large Sparse Systems of Equations*, Springer, 1993.

[11] S. Haker, A. Tannenbaum, and R. Kikinis, *Mass Preserving Mappings and Image Registration*, MICCAI 2001, pp. 120–127.

[12] S. Henn and K. Witsch, *Iterative Multigrid Regularization Techniques for Image Matching*, SIAM J. Sci. Comput. (SISC), Vol. 23, No. 4, pp. 1077–1093, 2001.

[13] S. Henn, *A Multigrid Method for a Fourth-Order Diffusion Equation with Application to Image Processing*, SIAM J. Sci. Comput. (SISC), Vol. 27, No. 3, pp. 831–849, 2005.

[14] K. Höllig, *Finite Element Methods with B-Splines*, Frontiers in Applied Mathematics 26, SIAM, 2003.

[15] B.K.P. Horn and B.G. Schunck, *Determining Optical Flow*, Artif. Intell., Vol. 23, pp. 185 – 203, 1981.

[16] S.L. Keeling, *Image Similarity Based on Intensity Scaling*, submitted to the Journal of Mathematical Imaging and Vision.

[17] S.L. Keeling, *Geometric Multigrid for Generalized Affine and Generalized Rigid Image Registration*, submitted to the Journal of Mathematical Imaging and Vision.

[18] S.L. Keeling, *Medical Image Registration and Interpolation by Optical Flow with Maximal Rigidity*, *Mathematical Methods in Registration for Applications in Industry and Medicine*, O. Scherzer, ed., Mathematics in Industry, Springer Series, to appear.

[19] S.L. Keeling and G. Haase, *Geometric Multigrid for High-Order Regularizations of Early Vision Problems*, to appear in Applied Mathematics and Computation.

[20] S.L. Keeling and W. Ring, *Medical Image Registration and Interpolation by Optical Flow with Maximal Rigidity*, Journal of Mathematical Imaging and Vision, Vol. 23, No. 1, pp. 47–65, July 2005.

[21] M. Lefébure and L.D. Cohen, *Image Registration, Optical Flow and Local Rigidity*, Journal of Mathematical Imaging and Vision, Vol. 14, No. 2, pp. 131–147, March 2001,

[22] J.A. Little, D.L.G. Hill, and D.J. Hawkes, *Deformations Incorporating Rigid Structures*, Computer Vision and Image Understanding, Vol. 66, No. 2, pp. 223–232, 1997.

[23] F. Maes, A. Collignon, D. Vandermeulen, G. Marchal, and P. Suetens, *Multimodality Image Registration by Maximization of Mutual Information*, IEEE Trans. Med. Imaging, Vol. 16, pp. 187–109, 1997.

[24] J. Modersitzki, *Numerical Methods for Image Registration*, Oxford University Press, 2004.

[25] J. Modersitzki, *FLIRT with rigidity - image registration with a local non-rigidity penalty*, IJCV, pp. 1–18, 2007.

[26] W. Peckar, C. Schnörr, K. Rohr and H.S. Stiehl, *Parameter-Free Elastic Deformation Approach for 2D and 3D Registration using Prescribed Displacements*, Journal of Mathematical Imaging and Vision, Vol. 10, pp. 143–162, 1999.

[27] D. Rueckert, B. Clarkson, D.L.G. Hill, D.J. Hawkes, *Non-rigid Registration using Higher-Order Mutual Information*, Medical Imaging 2000: Image Processing, K. M. Hanson, ed., Proceedings of SPIE, Vol. 3979, pp. 438–447, 2000.

[28] D. Rueckert, L.I. Sonoda, C. Hayes, D.L.G. Hill, M.O. Leach and D.J. Hawkes, *Non-rigid Registration using Free-Form Deformations: Application to Breast MR Images*, IEEE Trans. Med. Imaging, Vol. 18, No. 8, pp. 712–721, 1999.

[29] C. Studholme, D.L.G. Hill, D.J. Hawkes, *An Overlap Invariant Entropy Measure of 3D Medical Image Alignment*, Pattern Recognition, Vol. 32, pp. 71–86, 1999.

[30] P.M. Thompson, M.S. Mega, K.L. Narr, E.R. Sowell, R.E. Blanton and A.W. Toga, *Brain Image Analysis and Atlas Construction*, Medical Image Processing, Chapter 17 of Volume II of the Handbook of Medical Imaging, M. Sonka and J.M. Fitzpatrick, ed., SPIE Press (July, 2000).

[31] P.A. Viola, *Alignment by Maximization of Mutual Information.*, Ph.D. thesis, Massachusetts Institute of Technology, 1995.

[32] W.M. Wells, P. Viola, H. Atsumi, S. Nakajima, and R. Kikinis, *Multi-modal Volume Registration by Maximization of Mutual Information*, Med. Image Anal., Vol. 1, pp. 35–51, 1996.

[33] J. B. West, J. M. Fitzpatrick, M. Y. Wang, B. M. Dawant, C. R. Maurer, Jr., R.M. Kessler, R.J. Maciunas, C. Barillot, D. Lemoine, A. Collignon, F. Maes, P. Suetens, D. Vandermeulen, P.A. van den Elsen, S. Napel, T.S. Sumanaweera, B. Harkness, P.F. Hemler, D.L.G. Hill, D.J. Hawkes, C. Studholme, J.B.A. Maintz, M.A. Viergever, G. Malandain, X. Pennec, M.E. Noz, G.Q. Maguire, Jr., M. Pollack, C.A. Pelizzari, R.A. Robb, D. Hanson, and R.P. Woods, *Comparison and Evaluation of Retrospective Intermodality Brain Image Registration Techniques*, J. Comput. Assist. Tomogr., Vol. 21, pp. 554–566, 1997.

[34] J. Weickert, A. Bruhn, N. Papenberg and T. Brox, *Variational Optical Flow Computation: From Continuous Models to Algorithms*, Otmar Scherzer (ed): Mathematical Method for Registration and Applications to Medical Imaging, Mathematics in Industry, Springer, Vol. 10, 2006.